Materials Views
www.MaterialsViews.com

ADVANCED
FUNCTIONAL
MATERIALS
www.afm-journal.de

FULL PAPER

Bioinspired Reversibly Cross-linked Hydrogels Comprising Polypeptide Micelles Exhibit Enhanced Mechanical Properties

Ali Ghoorchian, Joseph R. Simon, Bhuvnesh Bharti, Wei Han, Xuanhe Zhao, Ashutosh Chilkoti, and Gabriel P. López

Noncovalently cross-linked networks are attractive hydrogel platforms because of their facile fabrication, dynamic behavior, and biocompatibility. The majority of noncovalently cross-linked hydrogels, however, exhibits poor mechanical properties, which significantly limit their utility in load bearing applications. To address this limitation, hydrogels are presented composed of micelles created from genetically engineered, amphiphilic, elastin-like polypeptides that contain a relatively large hydrophobic block and a hydrophilic terminus that can be cross-linked through metal ion coordination. To create the hydrogels, heat is firstly used to trigger the self-assembly of the polypeptides into monodisperse micelles that display transition metal coordination motifs on their coronae, and subsequently cross-link the micelles by adding zinc ions. These hydrogels exhibit hierarchical structure, are stable over a large temperature range, and exhibit tunable stiffness, self-healing, and fatigue resistance. Gels with polypeptide concentration of 10%, w/v, and higher show storage moduli of ≈1 MPa from frequency sweep tests and exhibit self-healing within minutes. These reversibly cross-linked, hierarchical hydrogels with enhanced mechanical properties have potential utility in a variety of biomedical applications.

1. Introduction

Advances in molecular biology and synthetic chemistry have enabled the development of engineered proteins and polymers that are finding their way into a variety of applications in medicine and biotechnology,[1] from pharmaceuticals,[2] and regenerative medicine[3] to separations[4] and biosensing.[5] Hydrogels based on engineered peptides and proteins, termed biohydrogels, herein, are being studied extensively because of their biocompatibility and the ease with which biofunctionality—typically incorporated as one or more copies of a fused bioactive protein or peptide—can be encoded into these systems at the genetic level.[1a,6] The majority of efforts to engineer biohydrogels have focused on creating covalently cross-linked networks because of their mechanical stability.[7] Covalently cross-linked biohydrogels, however, are not always ideal because of i) their often complex synthesis, which in some cases results in the formation of toxic by-products from the cross-linking reaction, and ii) their inherently static and nonreversible cross-links.[8] This irreversibility can impede the remodeling of these hydrogels in a biological environment, and in vivo can potentially lead to cell death, induction of inflammatory responses, and ultimately failure of implanted devices.[7,9]

As an alternative, efforts have focused on the synthesis of biohydrogels based on noncovalent—electrostatic, hydrophobic, ionic, coordination or hydrogen-bonded—cross-linking.[7] These intermolecular interactions are generally reversible, are not typically associated with toxic by-products, and can result in facile hydrogel formation, good biocompatibility, and the potential for dynamic remodeling.[10] However, most of the noncovalently cross-linked biohydrogels reported to date are mechanically weak,[7,11] unstable, and can be permanently damaged even when they are subjected to relatively low forces, attributes which limit their use in many in vivo applications. These limitations have been circumvented to a certain extent in non-peptide-based hydrogels by the design of double-network hydrogels,[12] hydrogels made of polymers mixed with inorganic nanoparticles,[13] and use of self-assembling hierarchical structures, including micelles.[14–16]

Dr. A. Ghoorchian, J. R. Simon, W. Han,
Prof. A. Chilkoti, Prof. G. P. Lopez
NSF Research Triangle Materials Research Science
and Engineering Center
Department of Biomedical Engineering
Duke University
Durham, NC 27708, USA
E-mail: gabriel.lopez@duke.edu
Dr. B. Bharti
NSF Research Triangle Materials Research Science
and Engineering Center
Department of Chemical and Biomolecular Engineering
North Carolina State University
Raleigh, NC 27607, USA
Prof. X. Zhao
Soft Active Materials Laboratory
Department of Mechanical Engineering
Massachusetts Institute of Technology
Cambridge, MA 02139, USA
Prof. X. Zhao
NSF Research Triangle Materials Research Science
and Engineering Center
Department of Mechanical Engineering and Materials Science
Duke University
Durham, NC 27708, USA

FULL PAPER

During the past decade, several groups have studied the use of polymeric micelles as a means to introduce order and functionality into hydrogels using a variety of materials and cross-linking techniques.[13–15,17] In early work, polymeric micelles formed from synthetic block copolymers were immobilized on surfaces to induce anti-fouling functionality to the surface. Later, micellar particles were used as an additive to a polymeric hydrogel without affecting the cross-linking mechanism, with the aim of introducing drug loading capability to the gels.[18] Micellar hydrogels[18b,19] are a class of reversibly cross-linked materials that exhibit interesting rheological behavior in which control over their viscoelastic response can be useful in rheological modification for coating applications.[15] Almost all of these prior studies have used self-assembling synthetic polymers as the building blocks of micellar gels and the mechanical characteristics of these gels have thus far not been on par with the mechanical properties of naturally derived hierarchically structured gel-like materials.[15,20] Hartgerink et al.[21] used engineered polypeptides instead of synthetic polymers to make cylindrical micelles that were then covalently cross-linked into a biohydrogel scaffold to promote hydroxyapatite growth, but did not show enhanced mechanical properties prior to mineralization. Wright et al.[22] studied morphological characteristics of hydrogels made from hydrophobic interactions between genetically engineered amphiphilic elastin-like polypeptides (ELPs) and revealed the filamentous microstructure of such gels but did not investigate their mechanical properties.

We describe here a bioinspired, engineered polypeptide that can be reversibly cross-linked into a micellar hydrogel—a MiGel—with enhanced mechanical properties. It is inspired by the following design elements found in biological materials: 1) macromolecular subunits that 2) self-organize at the nanoscale[23] 3) into a hierarchical organization that yields a reversible network structure that gives rise to enhanced mechanical properties.[23,24] Examples of such materials include collagen,[25] actin microfilaments,[26] and microtubules.[27] At the lowest dimensional scale, the building block of the MiGel is an environmentally responsive, diblock polypeptide that can be thermally triggered to self-assemble into spherical micelles. The diblock polypeptide is designed with a transition metal binding peptide at the hydrophilic terminus of the polypeptide, such that a high density of metal coordination sites is presented on the coronae of the micelles. At the second level of hierarchical structure, these micelles are reversibly cross-linked through metal coordination bonds into a higher order structure—a macroscopic hydrogel. We chose metal coordination for reversible cross-linking as it is exploited by Nature for noncovalent, reversible organization of biological structures,[28] such as cross-linked byssal threads—strong, stiff structural fibers used by mussels to attach to rocks and other substrata.[29]

To create these hierarchical materials, we first use heat to trigger the self-assembly of recombinant polypeptides into monodisperse micelles that display transition metal coordination motifs on their coronae. We show that a MiGel is rapidly formed by the addition of Zn^{2+} to a colloidal suspension of the micelles. The hydrogel is stabilized by van der Waals and hydrophobic interactions in the core of the micelles, and by reversible metal coordination between micelles. In comparison to previously reported noncovalently cross-linked hydrogels,

such MiGels exhibit very high moduli and, once formed, can be reversibly disassembled to their micellar components through the addition of a strong metal ion chelator. Further, MiGels can rapidly self-heal and their stiffness can be tuned by changing the polypeptide concentration. This new bioinspired method for creating robust, hierarchically ordered biomaterials can be used to generate new platforms for a variety of biomedical applications such as tissue engineering, drug delivery, wound dressings, and biosensing.

2. Results and Discussion

2.1. Molecular Design of MiGels

The recombinant peptide system that we designed to assemble into a hierarchical hydrogel has two components. The first element is a diblock copolymer of an ELP. ELPs are a family of stimulus-responsive peptide polymers consisting of repeats of the VPGXG peptide motif, in which the identity of amino acid, X, the molecular weight of the polymer,[30] and its architecture,[31] determine the temperature- and salt-dependent hydrophobicity of the polypeptide. ELPs exhibit lower critical solution temperature (LCST) transition behavior,[32] and the phase transition temperature of ELPs can be tuned by their composition and chain length[30] or by changing environmental conditions such as ELP concentration and the type and concentration of the salt in an ELP solution.[30,33] ELPs are excellent candidates as building blocks for the design of hierarchical hydrogels because i) they are genetically encodable, which allows enormous control in their design, ii) they express at high yields in bacterial hosts,[33b] and iii) they can be purified easily by exploiting their LCST phase behavior.[34] The latter two features enable gram-scale quantities to be easily obtained, which is critical for the fabrication of hydrogels. Chilkoti and co-workers[35] have extensively investigated diblock ELPs that self-assemble into micelles, providing a body of knowledge that can be used in the design of polypeptides as building blocks for the fabrication of micellar hydrogels.

Diblock ELPs form micelles above a critical micellization temperature that is controlled by the hydrophobic block composition.[35a] Here, we refer to these constructs as micelle-forming (MF) ELPs, and in this study we formed a MF-ELP by fusing a relatively hydrophobic block (($VPGVG)_{60}$) to a more hydrophilic block (($VPGAGVPGGG)_{30}$). An ELP that has a similar composition and chain length as the MF-ELP, but where the amino acids are not arranged in a diblock architecture (termed the non-micelle-forming- (NMF-) ELP) was also synthesized as a negative control for the effect of micellization on network assembly. The NMF-ELP has the sequence ($VPGAGVPGGG)_{60}$.

The second design element in the recombinant peptide used to form hierarchical hydrogels is a transition metal-binding peptide that is presented at the hydrophilic terminus of the MF-ELP (**Figure 1**A) and the NMF-ELP (Figure S1, Supporting Information). We chose a peptide with an amino acid sequence (HEDGHWDGSEHGY) taken from the consensus zinc-binding sequence found in the active sites of matrix metalloproteinases.[36,37] Although many transition metal-binding peptides are available, we specifically choose a peptide that binds Zn^{2+}
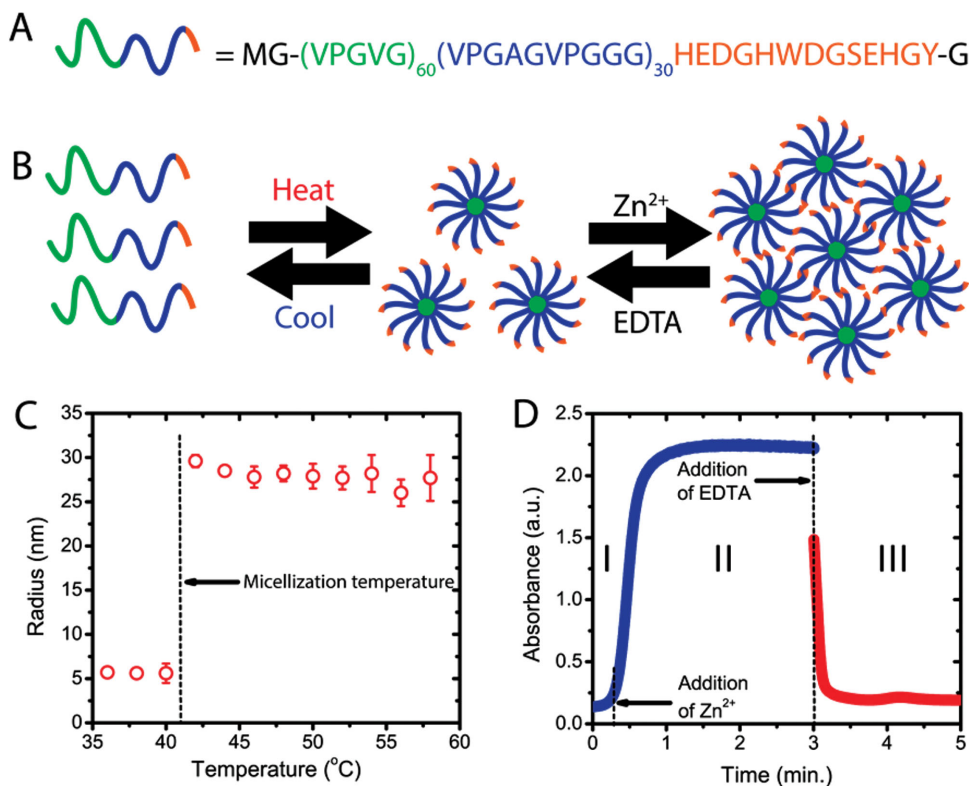
Figure 1. Thermally triggered assembly of MF-ELP into micelles and subsequent network formation. A) Amino acid sequence of the micelle-forming- (MF-) ELP. B) Schematic of temperature-triggered micellization of the diblock ELPs, metal-directed assembly of the micelles into a metal coordination stabilized network by addition of zinc ions, and disassembly of the network by the addition of EDTA. C) Hydrodynamic radius (R_h) of the MF-ELP (100×10^{-6} M, 0.5%, w/v) as a function of solution temperature, measured by DLS. D) Optical density at 350 nm of a solution of MF-ELP (100×10^{-6} M at 40 °C) indicating micelles (region I), network formation by addition of Zn^{2+} (region II), and disassembly back into micelles upon addition of EDTA (region III).

because, in contrast to Ni^{2+} and Cu^{2+}, Zn^{2+} is significantly less toxic, with a physiological concentration of 20×10^{-6} M[38] and a maximum tolerated concentration of 200×10^{-6} M in systemic circulation.[39]

2.2. Formation and Characterization of Micelles in Suspension

2.2.1. Micelle Assembly and On-demand Network Formation/ Dissolution

A schema that depicts micelle formation, network formation from micelles upon addition of Zn^{2+}, and network disaggregation back into micelles upon chelation of the Zn^{2+} ions is shown in Figure 1B. We first characterized the MF-ELP and NMF-ELP in a dilute aqueous solution (100×10^{-6} M, 0.5%, w/v) and in the presence of Zn^{2+}. Below the micellization temperature ($T_{micelle}$), the MF-ELP is not sufficiently amphiphilic to undergo self-assembly. Above its $T_{micelle}$, the preferential desolvation of the more hydrophobic block relative to the more hydrophilic block imparts sufficient amphiphilicity to drive self-assembly of the MF-ELP into micelles. The temperature-triggered assembly of the MF-ELP into micelles was confirmed by dynamic light scattering (DLS) (Figure 1C). The hydrodynamic radius (R_h) of the MF-ELP below its $T_{micelle}$ of ≈41 °C is ≈5 nm, which is consistent with other reports for random coil polypeptides.[40]

Above the $T_{micelle}$ of the MF-ELP, the R_h of the MF-ELP increases to ≈25–30 nm, which is also consistent with previous reports of micelles consisting of ELP diblock copolymers.[35a,40c,41] In contrast, the NMF-ELP forms large particles (>1 μm) as the temperature is raised above ≈40 °C (Figure S2, Supporting Information).

Addition of Zn^{2+} ions results in the cross-linking of the micelles formed from 100×10^{-6} M (0.5%, w/v) MF-ELP into large gel particles. Solutions containing these aggregates have a significantly higher optical density than solutions of non-aggregated micellar particles (Figure 1D). Micelle aggregation can be reversed by adding a chelating agent such as ethylenediaminetetraacetic acid (EDTA) due to its high affinity for zinc ions. Addition of EDTA to a solution of aggregated micelles at temperatures above the micellization temperature results in a rapid drop in the solution optical density to its pre-aggregation level, which suggests disaggregation to the original discrete micellar state (Figure 1D).

2.2.2. Characterization of Micelles by Light Scattering

To further investigate the size, shape, and aggregation number of the micelles formed from the MF-ELP, we examined the self-assembled nanostructures formed from MF-ELP by DLS and static light scattering (SLS) at different angles at a solution

FULL PAPER

Table 1. Hydrodynamic radius (R_h from DLS) and molecular weight (M_w), radius of gyration (R_g) and micelle aggregation number (from SLS) of micelles formed from MF-ELP for three different concentrations at 42 °C.

| Concentration [μM]	25	50	100
R_h [nm]	22 (±3.3%)	24 (±3.4%)	24 (±1.5%)
R_g [nm]	16 (±3.6%)	19 (±4.4%)	18 (±6.3%)
M_w [g mol^{-1}]	1.325 × 10^6 (±1.0%)	2.794 × 10^6 (±1.0%)	3.021 × 10^6 (±0.6%)
Aggregation number	15	23	25

temperature above the $T_{micelle}$. At three different concentrations (25 × 10^{-6}, 50 × 10^{-6}, and 100 × 10^{-6} M, i.e., 0.125%, 0.25%, and 0.5%, w/v), the MF-ELP forms micelles with a R_h of ≈23 nm as measured by DLS at angles ranging from 30° to 150° (Figure S3, Supporting Information, **Table 1**). The relatively constant size of the micelles measured at different angles suggests that they are spherical.[42] We also conducted SLS measurements to measure the radius of gyration (R_g) and molecular weight (M_w) of the micelles formed at the three different concentrations (Figure S4, Supporting Information, Table 1). The radii of gyration of the micelles measured at these concentrations range from 15 to 22 nm (Table 1), which is slightly smaller than R_h, as expected for spherical particles.[42,43] The ratio of R_g to R_h for different concentrations ranges from 0.72 to 0.79, which also suggests the existence of "hard spheres" in solution.[42] As the MF-ELP is monodisperse with a molecular weight of 48.6 kDa, we can estimate the average number of the polypeptide chains in each micelle (i.e., the aggregation number). The aggregation number is corrected for the amount of water trapped in the micelles by considering the water content of each micelle to be similar to that in ELP coacervates, which has been determined to be roughly 60% of the coacervate volume.[32] Using this assumption, we estimate the number of chains in each micelle to be ≈20, which also corresponds to the number of cross-linking motifs displayed on the corona of a single micelle.

2.3. Formation of MiGels

We made hydrogels containing 5%, 10%, and 15% w/v MF-ELP by adding zinc sulfate to a polypeptide solution to result in a 7.5 to 1 molar ratio of Zn^{2+} ions to peptide-binding sites. The temperature of the polypeptide solutions was kept at 45 °C (above the micellization temperature of the MF-ELP, but below the transition temperature for bulk aggregation) to ensure micelle formation before cross-linking. Addition of zinc sulfate to the solution of the MF-ELP resulted in rapid formation of a gel (**Figure 2**A). The hydrogels were kept at the same temperature for several hours to allow complete cross-linking and were subsequently centrifuged briefly to remove air bubbles before characterization. After cross-linking, the hydrogels were stable at room temperature, which is below the $T_{micelle}$ of ≈41 °C. This stability likely results from a decrease in the $T_{micelle}$ in the presence of zinc sulfate so that the micelles are stable at room temperature.[33b] To test this hypothesis, we added zinc sulfate (or sodium sulfate) to MF-ELP at room temperature and observed an increase in optical density characteristic of the

formation of micelles (Figure S5, Supporting Information).

For solutions of NMF-ELP on the other hand, the optical density profile as a function of temperature did not change appreciably in the presence of monovalent (Na$^+$) of divalent (Zn^{2+}) metal ions (Figure S2A, Supporting Information). DLS of the NMF-ELP also showed that the presence of Zn^{2+} ions had little impact on the size of the aggregates as a function of temperature compared to
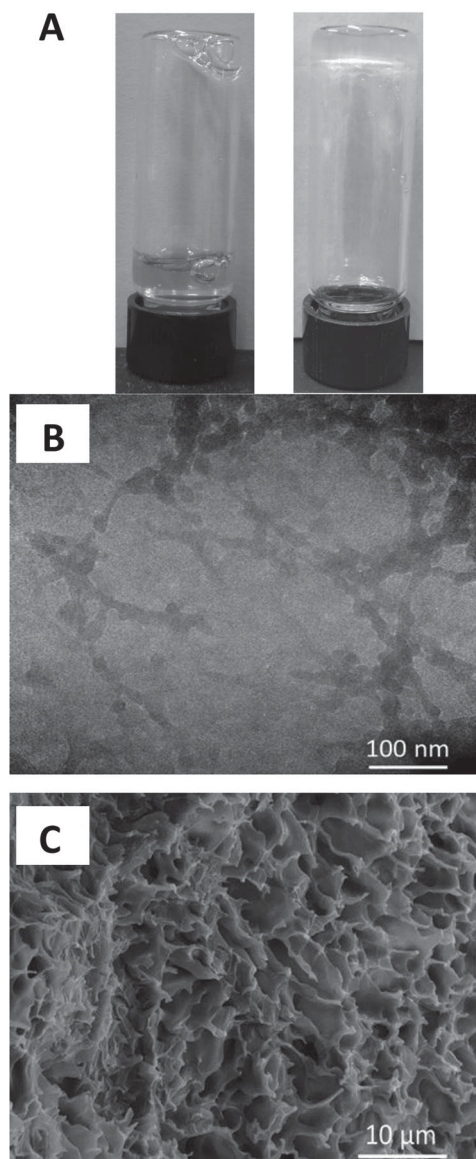
Figure 2. Formation of a hydrogel (MiGel) from MF-ELP and characterization of its microstructure by electron microscopy. A) Images of MF-ELP (10%, w/v) in micellar suspension before cross-linking (left) and after cross-linking by addition of zinc sulfate (20 × 10^{-3} M) to form a hydrogel (right). B) Cryo-TEM of incipient network (1% w/v MF solution frozen 10 s after addition of zinc sulfate (2 × 10^{-3} M). C) SEM of a freeze-dried mature MiGel (10% w/v MF-ELP, 20 × 10^{-3} M zinc sulfate).

www.MaterialsViews.com

ADVANCED
FUNCTIONAL
MATERIALS
www.afm-journal.de

FULL PAPER

the same ELP in water (Figure S2B, Supporting Information). Further, addition of zinc sulfate to solutions of NMF-ELP above its transition temperature (≈40 °C) results in the formation of a typical ELP coacervate that does not show gel-like properties (Figure S8, Supporting Information). This indicates that the presence of ELP micelles is necessary for the formation of a percolated cross-linked network.

2.4. Characterization of MiGels

### 2.4.1. Electron Microscopy

We examined the microstructure of the hydrogels by cryogenic transmission electron microscopy (cryo-TEM) and scanning electron microscopy (SEM). Using cryo-TEM, we captured the initial stage of the gel formation process (10 s after addition of ZnSO$_4$) in a dilute (1%, w/v polypeptide) solution (Figure 2B). Cryo-TEM samples were more dilute than those typically used to form the MiGels (≥5 wt%) to enable visualization of the incipient network before crowding of the micelles; the molar ratio of cross-linker (Zn^{2+}) to MF-ELP was kept the same as that used to form MiGels at the higher concentrations. During the early stages of network formation, cryo-TEM micrographs reveal individual micelle-like particles (i.e., of size comparable to that measured by light scattering) that are interconnected in a web-like network. This is in clear contrast with cryo-TEM micrographs of NMF-ELPs at a similar stage after addition of zinc ions, for which no such network is evident (Figure S6, Supporting Information).

SEM of freeze-dried 10% w/v MiGels after maturation of the cross-linked network (12 h after addition of ZnSO$_4$) shows a porous internal structure with a pore size less than 10 μm (Figure 2C). This is in clear contrast with the SEM images of the corresponding NMF-ELP structures (Figure S6, Supporting Information), which did not show a similar porous structure, suggesting that the cross-linking of micelles is related to the development of macroporosity.

Together, cryo-TEM and SEM analyses demonstrate a fundamental difference in microstructure of the hydrated MF-ELP- and NMF-ELP-based materials. Although we are still investigating the mechanism of gel formation, we believe that the formation of relatively large pores observed in the MF-ELP hydrogels is a result of the cross-linking of intact micellar structures. In contrast, the NMF-ELP lacks the ability to form a well-defined hybrid network that includes both i) cross-links formed by hydrophobic and van der Waals interactions and ii) cross-links formed by the coordination of Zn^{2+}, and thus do not yield a hydrogel, but form a highly entangled coacervate above their transition temperature.

2.4.2. X-Ray Scattering

Figure 3 shows the small angle X-ray scattering (SAXS) profiles for three different MiGels formed at different concentrations of MF-ELP. The scattering intensity $I(q)$ is presented as a function of wave vector $q = (4\pi/\lambda)\sin\theta$, where $\lambda = 0.15418$ nm and 2θ is the scattering angle. At $q > 0.5$ nm^{-1}, the SAXS
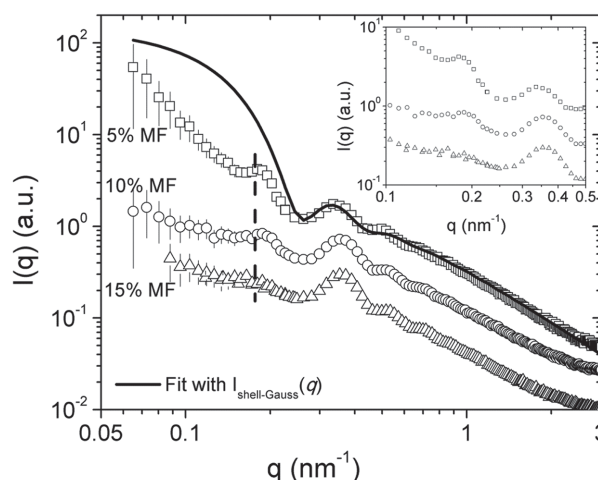
Figure 3. SAXS intensity profiles for MiGels formed at three different concentrations of MF-ELP. Squares: 5% w/v MiGel, circles: 10% w/v MiGel, triangles: 15% w/v MiGel; the data are offset for clarity of presentation. The solid black line represents the fit to 5% w/v MiGel SAXS profile at $q > 0.3$ nm^{-1} using the form factor of spherical shells and Gaussian chains ($I_{\text{shell-gauss}}$). The dashed line is a reference to indicate the shift in the inter-particle correlation peak for three gel concentrations (also shown as the inset).

profiles show $I(q) \propto q^{-2}$ dependency of scattering intensity, which is characteristic of polymer Gaussian chains. Modeling of the X-ray scattering data for the 5% w/v MiGel was carried out as described in the Supporting Information (see Table S1, Supporting Information, for fitting parameters), which also includes a brief discussion of scattering theory. In Figure 3, the discrete points are the experimental SAXS data and the solid line is the fit to the curve using a spherical core–shell model, as described in the Supporting Information. Scattering in the high q region, i.e., $q > 0.2$ nm^{-1}, reflects the signature of the size and shape of the self-assembled micelles in the hydrogel and is well represented by the core–shell form factor (for details see Supporting Information). The position of the form factor primary maxima ($q = 0.3$ nm^{-1}) does not change appreciably upon increasing the concentration of MF-ELP from 5% w/v to 15% w/v (Figure 3), indicating that the local geometry and structure of micelles in the hydrogels remain unaltered upon change in concentration. Core micelle radii of ≈15 nm were obtained for all MiGels examined, and are in reasonable agreement with the results of light scattering. No form-factor oscillation was observed for samples of NMF-ELP (Figure S7, Supporting Information).

The core–shell form factor model did not reproduce the maxima at $q \approx 0.18$ nm^{-1} observed for the MiGels (Figure 3). We believe that this peak corresponds to the spatial correlations between the micelles in the hydrogel phase. Direct fitting of this pseudo-order (or structure factor) peak is nontrivial. However, the correlation distance "D" between the micelles can be extracted from the location of peak maxima "q_c" using the relation: $D = 2\pi/q_c$.[44] **Table 2** summarizes the correlation distances between the micelles obtained for the three different polymer concentrations. The peak shifts to higher q values with increasing concentration (Figure 3 inset), corresponding to a decrease in the correlation distance for the micelles from 35 to

Table 2. Correlation distance (*D*) between the micelles in MiGels, as extracted from the X-ray scattering correlation peak, q_c. The distance ratio "r_D" and concentration ratio "r_c" are given with respect to the 5% w/v MiGel.

| Concentration (c) of polypeptide in MiGel [% w/v]	q_c [nm^{-1}]	D [nm]	$r_D = D/D_5$	$r_c = c^{1/3}/c_5^{1/3}$
5	0.18	34.9	1.0	1.0
10	0.20	31.4	1.1	1.2
15	0.26	24.1	1.4	1.4

24 nm. For the studied gel concentrations, we find that the distance scales as $D \propto \text{conc}^{1/3}$ (Table 1).

The scattering curve for a 5% w/v MiGel shows a steep increase in the scattering intensity at low *q*. This increase can be attributed to the interlinking of the micelles into larger structures.[4] However, this increase in intensity becomes less pronounced with increasing polymer concentration. It was not possible using X-ray scattering alone to determine the exact origin of this behavior. However, we speculate that two effects contribute to this decrease in scattering intensity at higher concentrations of MF-ELP. First, increasing concentration may lead to cross-linking of the micelles into denser networks and hence the scattering interface may become more diffuse. Second, the increase in polypeptide and Zn^{2+} concentrations might change the effective scattering length density of the interlinked Gaussian chains and the surrounding aqueous media. Similar effects have been observed by contrast variation in small angle neutron scattering experiments (SANS) for block copolymer micelles.[45] Further X-ray and neutron scattering studies would be necessary to confirm these effects, and are beyond the scope of this study. In summary, microstructural characterization with SAXS provides further evidence that hydrogels formed from MF-ELP comprise networks of intact, randomly packed micelles with spherical cores. This observation is in accordance with the theory of random packing of spheres, where the mean interparticle pair distance scales similarly.[46]

2.5. Mechanical Properties of MiGels

2.5.1. Rheological Studies

We studied the rheological behavior of MiGels at different concentrations of the MF-ELP (**Figure** 4A, S8, Supporting Information) and at room temperature (25 °C), which is above T_{micelle} at the concentrations of ZnSO$_4$ used (see Figure S5, Supporting Information) and hypothesized that forming networks with different cross-link densities would lead to the ability to tune the mechanical properties of MiGels. For MiGels formed from MF-ELP concentrations >5% (i.e., 10%, 15%, and 20% w/v), the storage and loss moduli are relatively independent of the angular frequency in a range from 0.1 to 100 s^{-1} (see Figure 4A for data for 10%, w/v). These hydrogels are viscoelastic materials exhibiting storage moduli that are one order of magnitude higher than the corresponding loss moduli. The storage moduli for the MiGels made from 10%, 15%, and 20% w/v MF-ELP are all ≈1 MPa, which is considerably higher than reported storage moduli of other noncovalently cross-linked hydrogels with similar polymer
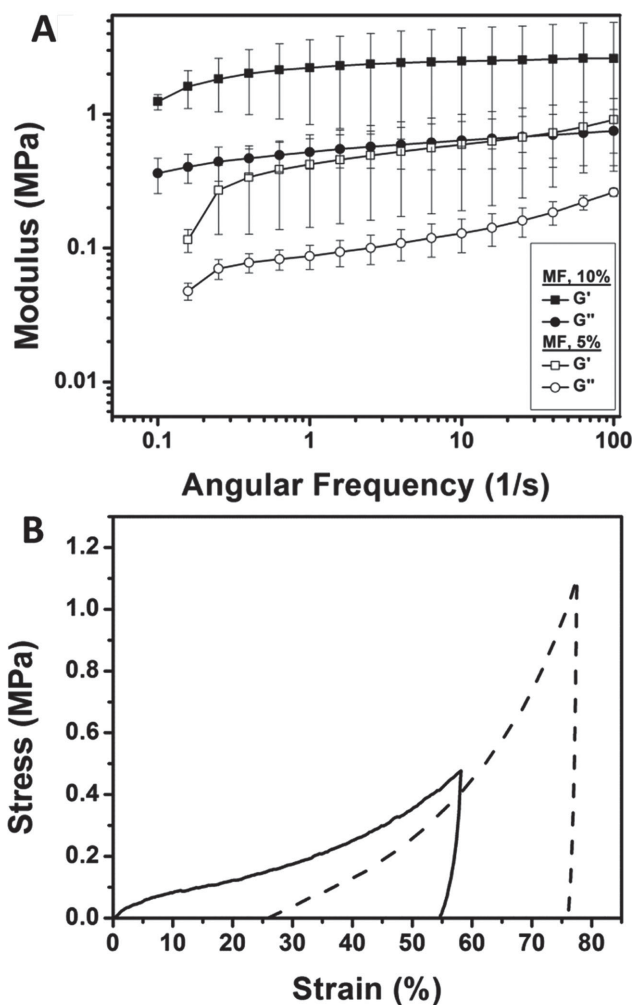
Figure 4. Mechanical characterization of MiGels. A) Storage and loss modulus for MiGels at 25 °C for two polymer concentrations (10% w/v, 5% w/v). Each point on the plot is an average value of three independent measurements and error bars are calculated standard deviations of the three measurements. B) Cyclic compression and expansion tests for MiGels (10% w/v) at 25 °C from 0% to 55% (solid line) and then immediately from 25% to 75% compressive strain (dashed line).

concentrations, including micellar hydrogels.[7,15,47] The storage modulus for 5%, w/v hydrogels is about an order of magnitude less than that of the 10%–20% w/v hydrogels. This indicates that tuning the moduli of the MiGels is possible by changing the MF-ELP concentration below 10% w/v.

The relatively high moduli of the MiGels may be due to a combination of structural factors, each of which individually has been shown to be effective in enhancing mechanical properties of micellar hydrogels. The hierarchical microstructure of the hydrogel may provide for especially efficient cross-linking.[48] The concentration of active stress-bearing sub-chains, derived from the kinetic theory of rubber elasticity, however, is greater than the concentration of peptide strands. In other words, an untangled polymer network of unit efficient cross-linking per se would not result in such a high modulus.[49] The hydrophobic cores of the micelles are aggregates of large hydrophobic

polypeptide chains within a minimal solution fraction, and it is possible that these aggregates can essentially function as highly entangled nodes throughout the gel. These micellar cores might function as especially stiff components that contribute considerably to the high modulus of the gels.[49] It is further notable that the MiGels are highly porous (Figure 2C), with pore sizes much larger than the hydrodynamic radii of the micelles. Also, fibrillar structures made from individual micelles are evident from cryo-TEM images of the incipient MiGel network (Figure 2B). This suggests that these gels are not comprised merely of agglomerations of micelles, but rather of filamentous structures of tightly connected micelles that form a network superstructure. Such a filamentous structure has been observed for ELP micelles before.[22] It has also been shown that hydrogels made of micelle-based filaments can show enhanced mechanical properties depending on their core size.[50] Efficient and perhaps synergistic combination of hydrophobic interactions and coordination chemistry, both of which have been shown to be effective in enhancing the mechanical characteristics of hydrogels, is likely key to imbuing the MiGels with mechanical robustness despite the lack of covalent cross-linking.[14,15,51]

In contrast, addition of zinc sulfate to NMF-ELP results in formation of materials with characteristics of a fluid with low moduli (Figure S9, Supporting Inforamtion). This is likely due to the fact that, in contrast to the MF-ELP, which can form network associations (i.e., cross-links) by both ion coordination and formation of micellar cores, the NMF-ELP only has one cross-linkable group and thus does not form a gel network.

2.5.2. Compression Tests

The MiGels did not show much stretchability (data not shown). We conducted unconfined compression tests on MiGels formed from a 10% w/v solution of the MF-ELP. The gels were cast into disks, and each disk was compressed to prescribed strains and then unloaded for two cycles. The gels undergo significant deformation during the compression tests (Figure 4B). Upon unloading, large hysteresis loops can be observed in the stress versus strain curves of the gels, which indicates significant energy dissipation due to the breaking and subsequent at least partial reformation of reversible cross-links. From the initial slope of the stress–strain curve, we can calculate the maximum compressive moduli of the MiGels, which is as high as ≈0.8–1.0 MPa. This compressive modulus is much higher than that of the NMF-ELP control (Figure S10, Supporting Information) and other biopolymer-based hydrogels.[11a,51b]

2.5.3. Self-Healing Properties

The reversibility of the cross-links that form the MiGel networks can enable spontaneous healing of the network after it
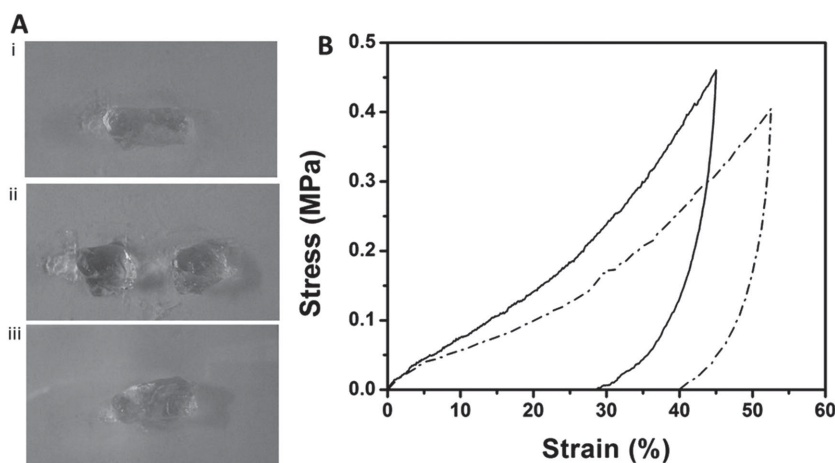
Figure 5. Self-healing of a MiGel. A-i) Picture of a virgin MiGel (10% w/v), A-ii) the MiGel after it has been severed into two pieces, and A-iii) the repaired MiGel about 1 min after the two pieces are put back together. B) Compressive stress response of the virgin (solid) and healed (dashed) MiGel (10% w/v).

has been disrupted. As shown in **Figure 5**A, the MiGels are able to self-adhere after they have been severed into two separate fragments. Inter- or intramicellar bonds are quickly (≈1 min) re-established when the surface of the two fragments is brought into close contact with one another. The reformed network exhibits similar mechanical properties as the native MiGel before disruption (Figure 5B). This MiGel self-healing process has a time scale on the order of few minutes. Such healing time is faster than many other self-healing hydrogels[52] and thus may enable rapid MiGel self-repair in applications involving fast mechanical disturbances.

3. Conclusion

We have designed a new type of hierarchical, reversibly cross-linked hydrogel that consists of ELP micelles that display a high density of a metal coordination peptide motif on their corona. Upon addition of Zn^{2+}, these micelles cross-link into stiff hydrogels with high porosity. The network is formed and held together through the cross-linking of the micelles' coronae via metal coordination bonds and by van der Waals and hydrophobic interactions in the cores of the micelles. The gels have higher storage modulus and compressive modulus compared to other similar biobased, noncovalently cross-linked hydrogels. These gels dissipate energy readily under compressive loading and they exhibit self-healing after network disruption due to the reversible nature of the cross-links comprising the network. These new "MiGels" have potential for use in a wide range of applications, including those in which biocompatibility, biostability, and high mechanical strength are needed in a single gel.

4. Experimental Section

Materials: The pET24+ expression vector was purchased from Novagen (Madison, WI). Restriction enzymes, ligation and dephosphorylation enzymes were purchased from New England Biolabs

(Ipswich, MA). BL21 *Escherichia coli* cells were purchased from Bioline (Taunton, MA). All salts were purchased from Alfa Aesar (Ward Hill, MA). *E. coli* cell cultures were grown in TB media purchased from MO BIO laboratories Inc. (Carlsbad, CA). DNA extraction kits, DNA gel purification kits and PCR purification kits were purchased from Qiagen Inc. (Germantown, MD). Lacey carbon TEM grids (300 mesh, copper with grid hole size of approximately 63 µm) were purchased from Ted Pella Inc.

ELP Gene Synthesis: ELP genes were constructed using the recursive directional ligation by plasmid reconstruction method (PRe-RDL), as described previously.[53] The genes for the MF-ELP, and NMF-ELP without the C-terminal Zn^{2+} binding peptide were available from a previous study.[35e] We modified these genes to append a C-terminal trailer that encodes for the Zn^{2+} peptide as described elsewhere.[54] In brief, we singly digested a modified pET24+ expression vector by BseRI restriction enzyme and ligated an annealed oligonucleotide coding for the metal-binding domain. We then digested this plasmid with BseRI and BglI restriction enzyme to produce a trailer "B cut"; we also digested the plasmid containing MF-ELP and NMF-ELP genes by AcuI and BglI restriction enzyme to produce a leader "A cut" sequence. We then ligated the leader and trailer sequence to produce the MF-ELP and NMF-ELP sequences containing metal-binding domain at their C-terminal. The final sequence of the MF and NMF-ELPs, which were confirmed by DNA sequencing, are: MF: M(VPGVG)$_{60}$(VPGAGVPGGG)$_{30}$HEDGHWDGS EHGY; NMF: M(VPGVGVPGAG)$_{60}$ HEDGHWDGSEHGY.

Gene Expression and ELP Purification: The ELP genes were transformed into chemically competent *E. coli* BL21 cells and incubated overnight. We used a single *E. coli* colony to inoculate a starter culture of sterilized TB media that was supplemented with kanamycin and then incubated the culture overnight at 37 °C and 220 rpm. The starter culture was used to inoculate sterilized TB media in 4 L flasks, each containing 1 L of media supplemented with 45 µg mL^{-1} of kanamycin. The media were incubated at 37 °C and 220 rpm for 6 to 8 h before inducing with 0.1×10^{-3} M IPTG. The cultures were then shaken for another 12 to 14 h at 37 °C before harvesting and centrifuging at 4 °C and 4000 rpm for 15 to 20 min. We purified the ELPs from the harvested cells by first lysing the cells by sonication for 3 min at pulses of 10 s on and 30 s off to prevent the solution from over heating and purified the ELPs from the soluble fraction of the cell lysate by inverse transition cycling (ITC), which has been described elsewhere in detail.[54]

ELP Characterization: The purity and molecular weight of the purified proteins were characterized by 10%–20% gradient Tris-Glycerol SDS-PAGE (Thermo Scientific, CA). The concentration of the ELP solution was determined by weighing the ELP after it had been lyophilized. We studied the thermal behavior and transition temperature of the constructs with or without metal ions and chelating agents using UV–vis spectroscopy (Cary 300, Agilent Technology) prior to hydrogel formation.

Hydrogel Formation: We made hydrogels from various concentrations of the MF-ELP by heating the sample to 45 °C, which is above $T_{micelle}$ but below the bulk aggregation temperature (cloud point temperature) of the ELP. We then added a solution of $ZnSO_4$, to make 7.5 to 1 molar ratio of Zn^{2+} to peptide-binding sites, to the heated samples and kept the solution at 45 °C for several hours to let the gels slowly settle to the bottom of the microcentrifuge tube. The solution was then gently centrifuged at 200 rpm for 30 s to remove any entrapped air bubbles. For NMF-ELP, we heated the solution slowly to temperatures close to the ELP transition temperature and then added $ZnSO_4$ to the solution and continued heating above the transition temperature. The remainder of the process was the same as for the MF-ELP.

Microstructural Characterization: Microstructures of hydrogels made from MF-ELP and NMF-ELP were evaluated by SEM, cryo-TEM, and X-ray scattering. SEM was performed using a FEI XL30 SEM-FEG instrument with a beam density between 10 and 15 kV. We prepared the samples by freeze-drying the hydrogels for 48 h and crushing them into small pieces to expose the internal surface of the hydrogel. The gel pieces were then sputter coated with gold and fixed on the SEM stage. Cryo-TEM imaging was performed on a FEI Tecnai G^2 Twin instrument and Gatan 626 cryogenic holder. The samples were vitrified using a FEI

Mark III Vitrobot above 45 °C and 100% humidity. The cross-linker and polypeptide solution were sequentially and rapidly added to the grid, the solution was blotted for 5 s, plunged into liquid ethane, and transferred to the TEM instrument under liquid nitrogen. X-ray scattering data were collected using a SAXSLab instrument (Ganesha model) with a point-collimated pinhole system and 2D configurable detector equipped with a Cu Kα X-ray source (wavelength, $\lambda = 0.15418$ nm) operating at 50 kV. We used 40 µL of the gels confined between two Kapton films with thickness of about 1 mm. The measurements were made at source-to-detector distances of 1080, 480, and 180 mm at three different angles covering the wave vector range $0.1 < q < 10$ nm^{-1}. The 2D scattered intensity was monitored using a CCD detector and the 2D data were radially averaged using SAXSGUI software. Further analysis and data fitting were performed using SASfit software package. Each measurement was repeated at least three times. Hydrodynamic radius was collected at different temperatures using a temperature-controlled DLS instrument (DynaPro, Wyatt Technologies). A 90° detector measured intensity fluctuations from below to above the micellization temperature by increasing the temperature in increments of 2 °C. R_g, R_h, and M_W of the MF-ELP and NMF-ELP constructs were calculated using SLS data at different angles that were obtained from an ALV/LSE-5004 SLS instrument equipped with a CGS3 compact goniometer system. We performed measurements on solutions of the ELPs at three different concentrations (25×10^{-6}, 50×10^{-6}, and 100×10^{-6} M) at a temperature above the $T_{micelle}$ of the MF-ELP ($\approx$41 °C).

Characterization of the Mechanical Properties of Hydrogels: The mechanical and rheological properties of the hydrogels were studied using an Anton Paar rheometer with temperature control and a humidity chamber. The gels were loaded on 8 mm standard steel parallel plates or 25 mm diameter cone-plates and frequency sweep experiments were done from 0.1 to 100 Hz with a 1% strain limit. Compression and release were studied of the MF gels on a micro-structure Analyzer (TA instrument). The gels were loaded on 8 mm standard steel parallel plates. The strain was changed with constant rate of 0.05 mm s^{-1} in positive and negative directions for compression and release tests.

Supporting Information

Supporting Information is available from the Wiley Online Library or from the author.

Acknowledgements

[1] a) E. F. Banwell, E. S. Abelardo, D. J. Adams, M. A. Birchall, A. Corrigan, A. M. Donald, M. Kirkland, L. C. Serpell, M. F. Butler, D. N. Woolfson, *Nat. Mater.* **2009**, *8*, 596; b) O. D. Krishna, K. L. Kiick, *Biopolymers* **2010**, *94*, 32; c) L. A. Reis, L. L. Y. Chiu, Y. Liang, K. Hyunh, A. Momen, M. Radisic, *Acta Biomater.* **2012**, *8*, 1022; d) A. Skerra, *J. Mol. Recognit.* **2000**, *13*, 167; e) C. G. Tate, G. F. X. Schertler, *Curr. Opin. Struct. Biol.* **2009**, *19*, 386.

[2] N. Chennamsetty, V. Voynov, V. Kayser, B. Helk, B. L. Trout, *Proc. Natl. Acad. Sci. U.S.A.* **2009**, *106*, 11937.

www.MaterialsViews.com

ADVANCED
FUNCTIONAL
MATERIALS
www.afm-journal.de

FULL PAPER

[3] B. V. Slaughter, S. S. Khurshid, O. Z. Fisher, A. Khademhosseini, N. A. Peppas, *Adv. Mater.* **2009**, *21*, 3307.

[4] J. R. Luther, C. E. Glatz, *Biotechnol. Bioeng.* **1994**, *44*, 147.

[5] a) R. Capone, S. Blake, M. R. Restrepo, J. Yang, M. Mayer, *J. Am. Chem. Soc.* **2007**, *129*, 9737; b) A. Hennig, G. J. Gabriel, G. N. Tew, S. Matile, *J. Am. Chem. Soc.* **2008**, *130*, 10338.

[6] S. Banta, I. R. Wheeldon, M. Blenner, *Annu. Rev. Biomed. Eng.* **2010** *12*, 167.

[7] C. Foo, J. S. Lee, W. Mulyasasmita, A. Parisi-Amon, S. C. Heilshorn, *Proc. Natl. Acad. Sci. U.S.A.* **2009**, *106*, 22067.

[8] W. E. Hennink, C. F. van Nostrum, *Adv. Drug Delivery Rev.* **2012**, *64*, 223.

[9] a) J. Berger, M. Reist, J. M. Mayer, O. Felt, N. A. Peppas, R. Gurny, *Eur. J. Pharm. Biopharm.* **2004**, *57*, 19; b) G. D. Nicodemus, S. J. Bryant, *Tissue Eng. Part B: Rev.* **2008**, *14*, 149.

[10] W. E. Hennink, C. F. van Nostrum, *Adv. Drug Delivery Rev.* **2002**, *54*, 13.

[11] a) J. A. Gustafson, R. A. Price, J. Frandsen, C. R. Henak, J. Cappello, H. Ghandehari, *Biomacromolecules* **2013**, *14*, 618; b) M. J. Reilly, *Colloids Surf. B* **2008**, *63*, 2, 269.

[12] J. Y. Sun, X. H. Zhao, W. R. K. Illeperuma, O. Chaudhuri, K. H. Oh, D. J. Mooney, J. J. Vlassak, Z. G. Suo, *Nature* **2012**, *489*, 133.

[13] a) W. C. Lin, W. Fan, A. Marcellan, D. Hourdet, C. Creton, *Macromolecules* **2010**, *43*, 2554; b) S. K. Agrawal, N. Sanabria-DeLong, G. N. Tew, S. R. Bhatia, *Langmuir* **2008**, *24*, 13148.

[14] D. C. Tuncaboylu, M. Sari, W. Oppermann, O. Okay, *Macromolecules* **2011**, *44*, 4997.

[15] J. Brassinne, A. M. Stevens, E. Van Ruymbeke, J. F. Gohy, C. A. Fustin, *Macromolecules* **2013**, *46*, 9134.

[16] M. J. Glassman, B. D. Olsen, *Soft Matter* **2013**, *9*, 6814.

[17] a) B. S. Kim, S. W. Park, P. T. Hammond, *ACS Nano* **2008**, *2*, 386; b) A. Laschewsky, P. Muller-Buschbaum, C. M. Papadakis, *Intelligent Hydrogels*, Vol. 140, (Eds: G. Sadowski, W. Richtering), Springer Switzerland **2013**, 15.

[18] a) L. Wei, C. H. Cai, J. P. Lin, T. Chen, *Biomaterials* **2009**, *30*, 2606; b) D. Ma, H. B. Zhang, K. Tu, L. M. Zhang, *Soft Matter* **2012**, *8*, 3665.

[19] a) P. Guillet, C. Mugemana, F. J. Stadler, U. S. Schubert, C. A. Fustin, C. Bailly, J. F. Gohy, *Soft Matter* **2009**, *5*, 3409; b) L. X. Xiao, J. H. Zhu, J. D. Londono, D. J. Pochan, X. Q. Jia, *Soft Matter* **2012**, *8*, 10233.

[20] B. D. Olsen, J. A. Kornfield, D. A. Tirrell, *Macromolecules* **2010**, *43*, 9094.

[21] J. D. Hartgerink, E. Beniash, S. I. Stupp, *Science* **2001**, *294*, 1684.

[22] E. R. Wright, V. P. Conticello, R. P. Apkarian, *Microsc. Microanal.* **2003**, *9*, 171.

[23] M. A. Meyers, P. Y. Chen, A. Y. M. Lin, Y. Seki, *Prog. Mater Sci.* **2008**, *53*, 1.

[24] S. Bechtle, S. F. Ang, G. A. Schneider, *Biomaterials* **2010**, *31*, 6378.

[25] M. Vanderrest, R. Garrone, *FASEB J.* **1991**, *5*, 2814.

[26] a) A. J. Maniotis, C. S. Chen, D. E. Ingber, *Proc. Natl. Acad. Sci. U.S.A.* **1997**, *94*, 849; b) A. McGough, B. Pope, W. Chiu, A. Weeds, *J. Cell Biol.* **1997**, *138*, 771.

[27] N. Mizuno, A. Narita, T. Kon, K. Sutoh, M. Kikkawa, *Proc. Natl. Acad. Sci. U.S.A.* **2007**, *104*, 20832.

[28] a) I. Massova, L. P. Kotra, R. Fridman, S. Mobashery, *FASEB J.* **1998**, *12*, 1075; b) F. Loechel, U. M. Wewer, *FEBS Lett.* **2001**, *506*, 65.

[29] J. H. Waite, X.-X. Qin, K. J. Coyne, *Matrix Biol.* **1998**, *17*, 93.

[30] D. E. Meyer, A. Chilkoti, *Biomacromolecules* **2004**, *5*, 846.

[31] A. Ghoorchian, N. B. Holland, *Biomacromolecules* **2011**, *12*, 4022.

[32] D. W. Urry, T. L. Trapane, K. U. Prasad, *Biopolymers* **1985**, *24*, 2345.

[33] a) D. E. Meyer, A. Chilkoti, *Biomacromolecules* **2002**, *3*, 357; b) Y. H. Cho, Y. J. Zhang, T. Christensen, L. B. Sagle, A. Chilkoti, P. S. Cremer, *J. Phys. Chem. B* **2008**, *112*, 13765.

[34] a) D. E. Meyer, A. Chilkoti, *Nat. Biotechnol.* **1999**, *17*, 1112; b) D. T. McPherson, C. Morrow, D. S. Minehan, J. G. Wu, E. Hunter, D. W. Urry, *Biotechnol. Prog.* **1992**, *8*, 347.

[35] a) M. R. Dreher, A. J. Simnick, K. Fischer, R. J. Smith, A. Patel, M. Schmidt, A. Chilkoti, *J. Am. Chem. Soc.* **2008**, *130*, 687; b) J. R. McDaniel, S. R. MacEwan, X. H. Li, D. C. Radford, C. D. Landon, M. Dewhirst, A. Chilkoti, *Nano Lett.* **2014**, *14*, 2890; c) D. J. Callahan, W. E. Liu, X. H. Li, M. R. Dreher, W. Hassouneh, M. Kim, P. Marszalek, A. Chilkoti, *Nano Lett.* **2012**, *12*, 2165; d) A. J. Simnick, M. Amiram, W. G. Liu, G. Hanna, M. W. Dewhirst, C. D. Kontos, A. Chilkoti, *J. Controlled Release* **2011**, *155*, 144; e) W. Hassouneh, K. Fischer, S. R. MacEwan, R. Branscheid, C. L. Fu, R. H. Liu, M. Schmidt, A. Chilkoti, *Biomacromolecules* **2012**, *13*, 1598.

[36] E. Hadler-Olsen, B. Fadnes, I. Sylte, L. Uhlin-Hansen, J. O. Winberg, *FEBS J.* **2011**, *278*, 28.

[37] W. Bode, F. X. Gomisruth, W. Stockler, *FEBS Lett.* **1993**, *331*, 134.

[38] K. Kasperek, L. E. Feinendegen, I. Lombeck, H. J. Bremer, *Eur. J. Pediatr.* **1977**, *126*, 199.

[39] P. Trumbo, A. A. Yates, S. Schlicker, M. Poos, *J. Am. Diet. Assoc.* **2001**, *101*, 294.

[40] a) J. Danielsson, J. Jarvet, P. Damberg, A. Graslund, *Magn. Reson. Chem.* **2002**, *40*, S89; b) A. Ghoorchian, K. Vandemark, K. Freeman, S. Kambow, N. B. Holland, K. A. Streletzky, *J. Phys. Chem. B* **2013**, *117*, 8865; c) A. Ghoorchian, J. T. Cole, N. B. Holland, *Macromolecules* **2010**, *43*, 4340.

[41] J. R. McDaniel, J. Bhattacharyya, K. B. Vargo, W. Hassouneh, D. A. Hammer, A. Chilkoti, *Angew. Chem. Int. Ed.* **2013**, *52*, 1683.

[42] W. Brown, *Dynamic Light Scattering: The Method and Some Applications*, Clarendon Press, Oxford **1993**.

[43] H. Kumari, S. R. Kline, J. L. Atwood, *Chem. Sci.* **2014**, *5*, 2554.

[44] B. Bharti, J. Meissner, G. H. Findenegg, *Langmuir* **2011**, *27*, 9823.

[45] J. S. Pedersen, C. Svaneborg, K. Almdal, I. W. Hamley, R. N. Young, *Macromolecules* **2003**, *36*, 416.

[46] S. Chandrasekhar, *Rev. Mod. Phys.* **1943**, *15*, 0001.

[47] a) K. J. Jeong, A. Panitch, *Biomacromolecules* **2009**, *10*, 1090; b) C. Q. Yan, D. J. Pochan, *Chem. Soc. Rev.* **2010**, *39*, 3528; c) J. T. Cirulis, F. W. Keeley, D. F. James, *J. Rheol.* **2009**, *53*, 1215; d) D. Asai, D. H. Xu, W. G. Liu, F. G. Quiroz, D. J. Callahan, M. R. Zalutsky, S. L. Craig, A. Chilkoti, *Biomaterials* **2012**, *33*, 5451; e) D. H. Xu, D. Asai, A. Chilkoti, S. L. Craig, *Biomacromolecules* **2012**, *13*, 2315; f) D. G. Abebe, T. Fujiwara, *Biomacromolecules* **2012**, *13*, 1828; g) V. Breedveld, A. P. Nowak, J. Sato, T. J. Deming, D. J. Pine, *Macromolecules* **2004**, *37*, 3943.

[48] T. Saito, T. Uematsu, S. Kimura, T. Enomae, A. Isogai, *Soft Matter* **2011**, *7*, 8804.

[49] C. R. Rubinstein, M, *Polymer Physics*, Oxford University Press, UK **2012**.

[50] L. H. Beun, I. M. Storm, M. W. T. Werten, F. A. de Wolf, M. A. C. Stuart, R. de Vries, *Biomacromolecules* **2014**, *15*, 3349.

[51] a) D. G. Barrett, D. E. Fullenkamp, L. H. He, N. Holten-Andersen, K. Y. C. Lee, P. B. Messersmith, *Adv. Funct. Mater.* **2013**, *23*, 1111; b) D. E. Fullenkamp, L. He, D. G. Barrett, W. R. Burghardt, P. B. Messersmith, *Macromolecules* **2013**, *46*, 1167.

[52] a) M. Guvendiren, H. D. Lu, J. A. Burdick, *Soft Matter* **2012**, *8*, 260; b) N. Holten-Andersen, M. J. Harrington, H. Birkedal, B. P. Lee, P. B. Messersmith, K. Y. C. Lee, J. H. Waite, *Proc. Natl. Acad. Sci. USA* **2011**, *108*, 2651; c) M. Nakahata, Y. Takashima, H. Yamaguchi, A. Harada, *Nat. Commun.* **2011**, *2*; d) M. M. C. Bastings, S. Koudstaal, R. E. Kieltyka, Y. Nakano, A. C. H. Pape, D. A. M. Feyen, F. J. van Slochteren, P. A. Doevendans, J. P. G. Sluijter, E. W. Meijer, S. A. J. Chamuleau, P. Y. W. Dankers, *Adv. Healthcare Mater.* **2014**, *3*, 70.

[53] J. R. McDaniel, J. A. MacKay, F. G. Quiroz, A. Chilkoti, *Biomacromolecules* **2010**, *11*, 944.

[54] W. Hassouneh, S. R. MacEwan, A. Chilkoti, *Methods in Enzymalogy* **2012**, *502*, 215.